

## Activity-Driven Phase Transition Causes Coherent Flows of Chromatin

Iraj Eshghi<sup>1</sup>, Alexandra Zidovska<sup>1</sup>, and Alexander Y. Grosberg<sup>1\*</sup>

*Center for Soft Matter Research, Department of Physics, New York University, New York, New York 10003, USA*



(Received 2 February 2023; accepted 23 June 2023; published 25 July 2023)

We discover a new type of nonequilibrium phase transition in a model of chromatin dynamics, which accounts for the coherent motions that have been observed in experiment. The coherent motion is due to the long-range cooperation of molecular motors tethered to chromatin. Cooperation occurs if each motor acts simultaneously on the polymer and the surrounding solvent, exerting on them equal and opposite forces. This drives the flow of solvent past the polymer, which in turn affects the orientation of nearby motors and, if the drive is strong enough, an active polar (“ferromagnetic”) phase of motors can spontaneously form. Depending on boundary conditions, either transverse flows or sustained longitudinal oscillations and waves are possible. Predicted length scales are consistent with experiments. We now have in hand a coarse-grained description of chromatin dynamics which reproduces the directed coherent flows of chromatin seen in experiments. This field-theoretic description can be analytically coupled to other features of the nuclear environment such as fluctuating or porous boundaries, local heterogeneities in the distribution of chromatin or its activity, leading to insights on the effects of activity on the cell nucleus and its contents.

DOI: [10.1103/PhysRevLett.131.048401](https://doi.org/10.1103/PhysRevLett.131.048401)

**Introduction.**—Chromatin is the functional form of DNA in living cells, with a variety of active processes such as transcription, replication, and DNA repair taking place directly on the chromatin fiber [1–3]. Active forces from these processes affect the organization and dynamics of chromatin [4–6]. Through displacement correlation spectroscopy, chromatin motions were simultaneously mapped across the entire nucleus in live cells, revealing that chromatin exhibits fast uncorrelated motions at short times ( $< 1$  s) and slow correlated motions at longer times [7]. The correlated chromatin motions are coherent over 3–5  $\mu\text{m}$  for several seconds, before the coherent domains break up and new ones form, resembling an oscillatorylike behavior [7]. Furthermore, while the uncorrelated motions were shown to be thermal-like, the coherent chromatin flows were eliminated upon ATP depletion or inhibition of major nuclear enzymes such as RNA polymerase II, DNA polymerase, and topoisomerase II, demonstrating the active, energy-dissipating and nonequilibrium nature of the coherent chromatin flows [7–9].

Hydrodynamics of systems with activity has been the subject of many studies in the context of active matter research, as reviewed in Ref. [10]. Depending on the role of solvent and the symmetry of the order parameter [11,12], active hydrodynamics exhibit phenomena ranging from coherent instabilities [13,14] to nematic or polar order [15–17] to treadmilling [18,19]. In many works, e.g., on active nematics, the idea is that nematic order is formed as in the usual passive system, due to interactions between, say, elongated molecules, and then activity drives spectacularly interesting dynamics (see Ref. [16]).

In the context of chromatin, unlike regular active nematics, molecular motors driving active dynamics, such as RNA polymerases, do not appear to be close enough to form a long-range order due to direct contact with each other [20]. At the same time, hydrodynamic treatment of chromatin finds that coherent dynamics can be sustained only in the presence of the ordered orientations of force dipoles [8]. In alternative hydrodynamics-free approaches, computationally reproducing coherent chromatin motions required the use of artificial long-range interactions [21–23]. An important hint came from hydrodynamic simulations work, where large-scale coherent chromatin dynamics as well as strong nematic order of chromatin fiber were observed, without inserting any artificial long-range forces [9]. Instead, this model relies on the nonspecific effects of hydrodynamics. In our earlier study, we identified motors, which exert equal but opposite forces on the polymer and solvent, as responsible for the large-scale hydrodynamic flows in the chromatin-nucleoplasm two-fluid system [24]. Here, we aim to develop a coarse-grained hydrodynamic model, which reproduces the development of the coherent chromatin phase. We hypothesize that there can be an ordering phase transition when the force of the motors exceeds a threshold value. We seek to analyze which properties of the chromatin-nucleoplasm system govern this phase transition as well as the structure of ordered phase.

**Model and equations of motion: Linear response.**—Following earlier work [8,24] we describe chromatin using the two-fluid model originally introduced by Doi and Onuki [25]. The dynamics of the system in this model is

described by the fields of polymer velocity  $\mathbf{v}^p(\mathbf{r}, t)$ , polymer volume fraction  $\phi(\mathbf{r}, t)$ , and the solvent velocity  $\mathbf{v}^s(\mathbf{r}, t)$ , while the solvent volume fraction is  $1 - \phi(\mathbf{r}, t)$  because of overall incompressibility. To describe the onset of spontaneous symmetry breaking and formation of polar ordered domains, we start with the assumption of linear and local rheological response of the polymer. This implies that the velocities are small, as are the deviations from the average density,  $\phi(\mathbf{r}, t) = \phi_0 + \delta\phi(\mathbf{r}, t)$ . This implies further that polymer osmotic pressure is  $\Pi \simeq K\delta\phi(\mathbf{r}, t)$ , with osmotic modulus  $K$ , while the force resulting from polymer viscous stress is  $\eta^p \star \nabla^2 \mathbf{v}^p(\mathbf{r}, t)$ , where polymer viscosity may have some time memory kernel and  $\star$  means convolution [see below about neglect of extensional viscosity and terms  $\sim \nabla(\nabla \cdot \mathbf{v}^p)$ ]. In this approximation, equations of motion of the model are conveniently written in the Fourier-transformed frequency domain (with sign convention  $\partial_t \rightarrow -i\omega$ ) as follows:

$$\zeta(\mathbf{v}_\omega^p - \mathbf{v}_\omega^s) = \eta_\omega^p \nabla^2 \mathbf{v}_\omega^p - K \nabla \delta\phi_\omega - \phi_0 \nabla P_\omega + \mathbf{F}_\omega^p, \quad (1a)$$

$$\zeta(\mathbf{v}_\omega^s - \mathbf{v}_\omega^p) = \eta^s \nabla^2 \mathbf{v}_\omega^s - (1 - \phi_0) \nabla P_\omega + \mathbf{F}_\omega^s, \quad (1b)$$

$$i\omega \delta\phi_\omega = \phi_0 \nabla \cdot \mathbf{v}_\omega^p = -(1 - \phi_0) \nabla \cdot \mathbf{v}_\omega^s. \quad (1c)$$

The first two equations represent force balance conditions for polymer and solvent, respectively, while the last two are continuity conditions for these two components. Here  $\zeta$  is the friction coefficient of polymer against solvent, per unit volume,  $\eta^s$  is the viscosity of the solvent,  $P_\omega$  is the hydrostatic pressure.

The heart of the problem is the understanding of active force densities  $\mathbf{F}^p$  and  $\mathbf{F}^s$  generated by motors. The typical size of every motor, which we denote  $a$ , is on the order of or smaller than the mesh size  $\lambda$ . As explained above, we focus on motors exerting equal and opposite forces on polymer and on solvent [Fig. 1(a)], which to the first approximation means  $\mathbf{F}^p = -\mathbf{F}^s = f\rho \mathbf{m}(\mathbf{r}, t)$ , where  $\rho$  is the number density of motors, while  $\mathbf{m}(\mathbf{r}, t) = \langle \hat{\mathbf{n}} \rangle$  is the average orientation. With  $f > 0$ , this describes extensile force dipoles; contractile ones correspond to  $f < 0$ . Remaining within linear response, we assume  $|\mathbf{m}|$  small and neglect the change of motor density associated with changing polymer density  $\delta\phi$ . Note that every motor has, generally, some finite processivity, stemming from its on and off rates; density  $\rho$  includes only those motors that are simultaneously working.

Since the body of the force-exerting motor is tethered to the polymer at one end and experiences friction from the solvent, there must be a torque acting on the motor and proportional to the relative velocity  $\mathbf{v}^p - \mathbf{v}^s = \mathbf{w}$ , leading to the following dynamics of the  $\mathbf{m}$  field (see Sec. I in Ref. [26]):

$$-i\omega \mathbf{m}_\omega = \frac{2}{3a} \mathbf{w}_\omega - 2 \frac{T}{\gamma} \mathbf{m}_\omega, \quad (2)$$

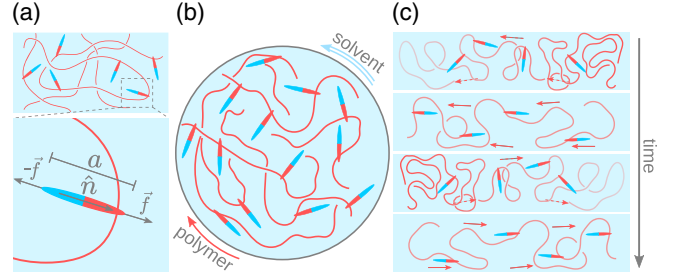


FIG. 1. Sketch of our model and the two dynamic modes. (a) Polymer with attached disordered motors; enlarged section shows one motor and its parameters. (b) Transverse mode in a spherical domain. Notice the polar alignment of motors. (c) Longitudinal, oscillatory mode. Time goes from the upper panel to the lower one, with time per frame given in Eq. (9). Dashed arrows show passive relaxation of polymer density. Solid arrows show the motor-driven polymer flow.

where  $\gamma$  is the rotational drag coefficient for the motor and  $T$  is the temperature in energy units.

Apart from nonlinearities (considered below), we neglect in Eq. (2) coupling of motor orientation to polymer concentration gradient (because motor size is smaller than or comparable to polymer mesh), do not consider renormalization of active force due to the flow itself (because  $f$  is large enough), and ignore the possibility of the induced nematicity of the polymer and corresponding active stress. Our theory is in some ways similar to that of Adar and Joanny [17], as they also examine coupling between flow and polarization in a two-fluid model, but they focus on the regime of strong polarization which can only rotate in response to the flow, while we concentrate on the chromatin-relevant opposite regime of weak polarization which only arises due to the flow.

Along with Eq. (2), it is convenient to recast the equations of motion (1) in terms of the above defined relative velocity  $\mathbf{w}_\omega = \mathbf{v}_\omega^p - \mathbf{v}_\omega^s$  and viscosity-weighted average velocity  $\mathbf{u}_\omega = (\eta_\omega^p \mathbf{v}_\omega^p + \eta^s \mathbf{v}_\omega^s) / (\eta_\omega^p + \eta^s)$  (see Sec. III in Ref. [26]). Doing so, one can see that relative velocity  $\mathbf{w}$  is driven by  $\mathbf{m}$ , i.e., mathematically by force monopoles rather than dipoles. A similar mathematical structure appeared in Ref. [44], albeit in a different physics context. This explains why hydrodynamic interactions are so important in our active system, despite the fact that in passive polymers they are screened at the distances not far exceeding the mesh size [45]. Another feature of the full set of equations is that they allow for simultaneous Helmholtz decomposition of the three vector fields  $\mathbf{m}$ ,  $\mathbf{u}$ , and  $\mathbf{w}$  to the uncoupled divergence-free (transverse,  $\perp$ ) and curl-free (longitudinal,  $\parallel$ ) modes.

*Threshold of instability: Divergence-free modes.*— Transverse modes do not involve density change,  $\delta\phi = 0$ , and, accordingly, no pressure gradient,  $\nabla P = 0$ . This leaves us with just two equations which are easily

combined into one (see Sec. III of Ref. [26]):

$$-i\omega\tau(1 - \lambda^2\nabla^2)\mathbf{w}_{\omega\perp} = 2\left(\frac{f\rho\gamma}{3a\zeta T} - 1 + \lambda^2\nabla^2\right)\mathbf{w}_{\omega\perp}, \quad (3)$$

where we introduced shorthand notations,

$$\tau = \frac{\gamma}{T} \quad \text{and} \quad \lambda^2 = \frac{\eta_{\omega}^p\eta^s/\zeta}{\eta_{\omega}^p + \eta^s} \simeq \frac{\eta^s}{\zeta}, \quad (4)$$

and in the last transformation we took into account the fact that  $\eta_{\omega}^p \gg \eta^s$ , by several orders of magnitude, over the entire frequency range of interest [27–35]. Clearly,  $\tau$  is the characteristic time of passive reorientation by a single motor, while  $\lambda$  is the length scale of the mesh size.

In an infinite domain, the modes are just plane waves,  $\nabla^2 \rightarrow -q^2$ , and we see that modes become unstable when  $(f\rho\gamma/3a\zeta T) - 1 > \lambda^2q^2$ . The fact that the length scale  $1/q$  of the unstable modes diverges as we approach from above the critical force level at which  $(f\rho\gamma/3a\zeta T) - 1 = 0$  is reminiscent of a second-order phase transition, similar to that in a magnet, with  $\mathbf{w}_{\perp}$  playing the role of (self-consistent) magnetic field and  $\mathbf{m}_{\perp}$  the local averaged spin. The critical parameter  $\epsilon = (f\rho\gamma/3a\zeta T) - 1$  describes a competition between the velocity produced by the cooperatively acting motors ( $f\rho/\zeta$ ) and the characteristic velocity needed to align a motor,  $aT/\gamma = a/\tau$ .

If the system is confined in a finite domain of size  $R$ , then modes have a more elaborate structure and discrete spectrum. Although the stability analysis for this case may require a separate study [46], the qualitative estimate of the amount of force needed to generate instability can be obtained by just setting  $q \sim 1/R$  (see Fig. 2):

$$f\rho > \frac{3a\zeta T}{\gamma} + \frac{a\eta_s T}{\gamma R^2}. \quad (5)$$

This condition means that motors acting together have to be strong enough to overcome the friction of the solvent pumped through the network (the first term) and additional friction against the boundary (the second term) [see Fig. 1(b)].

*Threshold of instability: Curl-free modes.*—The longitudinal waves involve density fluctuations, which is why their description is more complicated. Nevertheless, even in this case, the problem is reduced to a single equation for the field  $\mathbf{w}_{\parallel}$  (see Sec. III of Ref. [26] for derivation):

$$\begin{aligned} & [1 - \lambda_s^2\nabla^2]\tau^2\partial_t^2\mathbf{w}_{\parallel} - 4\lambda_d^2\nabla^2\mathbf{w}_{\parallel} \\ & + 2\left[1 - (\lambda_s^2 + \lambda_d^2)\nabla^2 - \frac{f\rho\gamma}{3a\zeta T}\right]\tau\partial_t\mathbf{w}_{\parallel} = 0, \end{aligned} \quad (6)$$

where in addition to Eq. (4) we introduced two new length scales; their complete expressions are cumbersome [see Eq. (26) in Ref. [26]], but in simplified form (due to

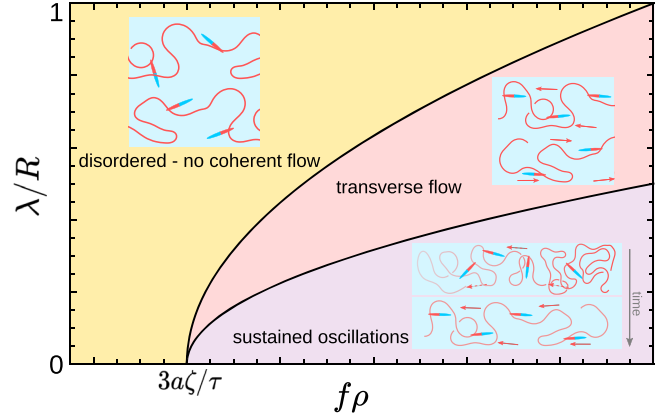


FIG. 2. Phase diagram of the instabilities and the regions of parameter space where they develop, as a function of the active force density and the size of the container. In the left (yellow) region of the diagram, the forcing is insufficient to drive instabilities and the system remains disordered. The middle (red) region is where the forces are sufficient to drive transverse flows but not strong enough to cause polymer density fluctuations. Finally, the bottom right (purple) region of parameter space is where both longitudinal oscillations and transverse flows are possible. The lines separating the regions correspond to the conditions in Eqs. (5) and (8), respectively.

$\eta_{\omega}^p \gg \eta^s$ ) they are as follows:

$$\lambda_s^2 \simeq \frac{\eta^p(1 - \phi_0)^2}{\zeta} \quad \text{and} \quad \lambda_d^2 \simeq \frac{K\phi_0(1 - \phi_0)^2\gamma}{2\zeta T}. \quad (7)$$

In Eq. (6), we returned to time domain ( $-i\omega \rightarrow \partial_t$ ), making the oscillator structure of the equation more transparent. This is possible only as long as polymer viscosity  $\eta_{\omega}^p$  is only smoothly dependent on frequency.

As in the transverse case before, in an infinite domain the modes are just plane waves,  $\nabla^2 \rightarrow -q^2$ , and Eq. (6) becomes that of a damped harmonic oscillator. Remarkably, active driving force comes only in the friction term. In particular, sufficiently strong and numerous motors can lead to the flipped sign of friction, making the oscillator unstable. As before, structure of modes for a finite size domain of size  $R$  requires special analysis [46], but qualitatively we can estimate the instability threshold by just replacing  $q \rightarrow 1/R$  (see Fig. 2):

$$f\rho > \frac{3a\zeta T}{\gamma} + \frac{(1 - \phi_0)^2 a}{R^2} \left[ \frac{3T\eta^p}{\gamma} + \frac{3}{2}K\phi_0 \right]. \quad (8)$$

Similar to the formula (5) for the transverse case, Eq. (8) means that motors have to be strong enough to overcome friction, which this time involves moving and deforming polymers, thus dependent on  $\eta^p$  and  $K$ , respectively. This implies that a larger force is needed to generate longitudinal modes compared to the transverse ones (and the extensional viscosity of the polymer can further increase this threshold).

When force is exactly equal to the threshold value for some  $q$ , this mode exhibits a sustained oscillation with frequency such that  $(\omega\tau)^2 = 2\lambda_d^2 q^2 / (1 + \lambda_s^2 q^2)$ . In particular, the small  $q$  modes ( $q\lambda_s \ll 1$ ) are just propagating waves with  $\omega \propto q$  and with velocity  $\sim \lambda_d / \tau \sim K/\zeta$ . Numerically generated movies illustrating possible wave packet dynamics can be found in Sec. IV of Ref. [26].

To rationalize this, let us define rate  $\tau_q^{-1} \sim (K/\zeta)q^2$ ; given that  $K/\zeta$  has dimensionality of a diffusion coefficient,  $\tau_q$  is the characteristic relaxation time of a density wave of length  $1/q$  by cooperative diffusion, driven by polymer elasticity ( $K$ ) against friction ( $\zeta$ ). In terms of  $\tau_q$ , we can write mode  $q$  frequency as the geometric mean of two rates:

$$\omega \sim (\tau\tau_q)^{-1/2}, \quad \text{with } \tau_q^{-1} \sim (K/\zeta)q^2. \quad (9)$$

The mathematical structure of frequency as the geometric mean of two rates is analogous to that which arises in the Lotka-Volterra equations [36,37], featuring the growth rate of the prey and the death rate of the predator. This structure reflects the physical nature of the oscillator: by the time some dense region of size  $1/q$  relaxes, it will have generated a velocity field which locally aligns the field  $\mathbf{m}_{\parallel}$ . This field has a persistence time  $\tau$ , and pumps the polymer in the same direction in which it was relaxing. This causes a new dense region to develop, until the dipoles lose their alignment in turn after a time  $\tau$ , and the polymer relaxation begins yet again at a rate  $1/\tau_q$  in the opposite direction. This is illustrated in Fig. 1(c).

If the force is slightly above or slightly below the threshold Eq. (8), then the oscillator is either slowly decaying (below) or slowly increase swinging (above), with characteristic time that diverges at the threshold, again reminiscent of a standard critical slowing-down in phase transitions.

*Beyond linear response.*—Once driving force exceeds the threshold value, unstable modes exponentially explode, grow out of the linear response range, and then nonlinearity comes to rescue and eventually arrests the growth. There are many nonlinear effects possible (see Sec. IIIC in Ref. [26]), but we will focus on the most basic and omnipresent one, namely, the fact that orientational order of motors is limited such that  $|\mathbf{m}| \leq 1$ : the maximum motors can do together is to align completely.

A complete description of orientation dynamics in an orienting field is rather cumbersome (see Sec. I in Ref. [26]). We will restrict ourselves with the simplest estimate, assuming that polarization vector  $\mathbf{m}$  beyond the linear regime Eq. (2) evolves according to

$$\begin{aligned} \tau\partial_t \mathbf{m} &= 2[\mathbf{m}_{\text{eq}}(\mathbf{w}) - \mathbf{m}], \\ \text{with } \mathbf{m}_{\text{eq}}(\mathbf{w}) &\simeq \mathbf{w} \frac{\tau}{3a} \left( 1 - \frac{(\mathbf{w}\tau/a)^2}{15} \right). \end{aligned} \quad (10)$$

Here  $\mathbf{m}_{\text{eq}}(\mathbf{w})$  is the equilibrium value that would be achieved in a constant flow  $\mathbf{w}$ ; similar to classical orientation of dipoles,  $m_{\text{eq}}(w) = \coth(w\gamma/aT) - aT/\gamma w$ , and we use the first nonlinear term of expansion. Equation (10) is not exact, but captures the main qualitative features.

Once the dynamics is nonlinear, separation of longitudinal and transverse modes is not possible. Nevertheless, neglecting frequency dependence of  $\eta^p$  (and, therefore,  $\lambda_s$ ), we can reduce equations of motion to a single equation (see Sec. III of Ref. [26]):

$$\begin{aligned} \tau^2 \partial_t^2 [1 - \lambda_s^2 \nabla \nabla \cdot + \lambda^2 \nabla \times \nabla \times] \mathbf{w} - 4[\lambda_d^2 \nabla \nabla \cdot] \mathbf{w} \\ + 2\tau \partial_t \left[ 1 - (\lambda_s^2 + \lambda_d^2) \nabla \nabla \cdot + \lambda^2 \nabla \times \nabla \times \right. \\ \left. - \frac{f\rho\gamma}{3a\zeta T} \left( 1 - \frac{\tau^2}{15a^2} \mathbf{w}^2 \right) \right] \mathbf{w} = 0. \end{aligned} \quad (11)$$

Equation (11) is instructive. First of all, if we drop the nonlinear term, then it is reduced to either Eq. (3) or Eq. (6) if the field  $\mathbf{w}$  is divergence-free or curl-free, respectively [47]. Of course, a full nonlinear equation is difficult to analyze. Nevertheless, Eq. (11) is still similar to that for an oscillator (specifically, the van der Pol oscillator [48,49]), with both active forces and nonlinear saturation contributing to the friction term (with first time derivative). All types of second spatial derivatives, arising from viscous stresses, are controlled by the domain size and estimated as  $1/R^2$ , although the detailed structure of the vector field  $\mathbf{w}$  is sensitive to the domain shape and boundary conditions. For an estimate, we just say that modes start to grow when force makes the friction term in Eq. (11) negative and then  $|\mathbf{w}|$  grows until the friction term becomes positive again. If the threshold for instability is  $(f\rho)^*$  [determined, e.g., by Eq. (8)], then the steady velocity amplitude scales as  $w^2 \sim (15a^2/\tau^2)[f\rho - (f\rho)^*]/(f\rho)^*$ , and the corresponding density variations amplitude is  $\delta\phi^2 \sim (15a^2\zeta/K\tau)[f\rho - (f\rho)^*]/(f\rho)^*$ . Numerical solutions are consistent with predicted scaling, as shown in Sec. IV of Ref. [26].

*Discussion.*—Our model predicts three phases for chromatin dynamics: disordered, and two types of polar order—transverse flows and oscillatory regime. These are controlled by the active force density  $f\rho$  and the domain size  $R$  (Fig. 2).

Our results are consistent with extensive simulations reported in Ref. [9], showing that extensile motors ( $f > 0$ ), if present in sufficient density  $f\rho$ , produce polar ordered state and coherent motion. An additional feature of the computational model [9] is that they observe nematic ordering of polymer itself; we speculate that nematicity of the polymer may be a consequence of the polar order of motors, because the motors in the simulations were tied to local direction of the polymer.

Speaking about chromatin *in vivo*, we consider RNA polymerase II as a likely motor driving chromatin

dynamics, as it binds to chromatin and pushes RNA into the solvent [1], although many other nuclear enzymes can also mechanically couple chromatin fiber to the nucleoplasm, e.g., loop extruding condensin [50]. For these motors, density  $\rho \gtrsim 10^2 \mu\text{m}^{-3}$  [38], force  $f \sim 25 \text{ pN}$  [51], size  $a \sim 20 \text{ nm}$  [52]. At full cooperation, when perfectly aligned, these motors can drive solvent past chromatin at a very large speed  $w_{\text{max}} \sim f\rho/\zeta \sim 10^7 \text{ nm/s}$ ; here, we used  $\zeta = \eta^s/\lambda^2$ , assuming nucleoplasm viscosity similar to that of water,  $\eta^s \sim 10^{-3} \text{ Pa s}$  [33,34], and taking chromatin mesh size  $\lambda \sim 50 \text{ nm}$  (30–100 nm reported in experiments [39,40]). Of course, polymer moves with a smaller speed, reduced by a factor of the ratio of viscosities,  $v^p \sim (\eta^s/\eta^p)w$ .

Unfortunately, the ratio of viscosities is difficult to measure directly. Using experimentally measured values of  $\eta^p$  and  $\eta^s$  [27–35], we estimate the ratio to be in the range  $10^{-2}$ – $10^{-6}$ . The latter figure would be in agreement with experimentally measured polymer speed in slow coherent motion about  $10 \text{ nm/s}$  [7]. If the actual ratio of viscosities is not quite that small, then we will have to conclude that chromatin *in vivo* operates close to criticality, where our model predicts reduction of velocity by a factor  $[f\rho/(f\rho)^* - 1]^{1/2}$ .

Can we estimate actual closeness to criticality, directly comparing force density to its critical value? The critical condition is given by  $f\rho/\zeta > (f\rho)^*/\zeta = (3a/\tau)[1 + \lambda^2/R^2]$ , Eq. (5). Here  $\lambda^2/R^2$  is negligible for realistic nucleus size of about  $R \sim 10 \mu\text{m}$  [1,3], but passive reorientation time of a motor  $\tau$  is yet another parameter poorly constrained by available experiments. We calculate  $\tau \gtrsim 10^{-6} \text{ s}$  (Sec. V of Ref. [26]), but the actual value could be significantly higher, since we underestimated the dissipative coupling between motor and polymer. Accepting our calculated value yields  $3a/\tau \lesssim 10^7 \text{ nm/s}$ , similar to  $w_{\text{max}}$  above. Thus, uncertainties in  $\tau$  and  $\eta^p/\eta^s$  are too great to find actual closeness to criticality. However, the known parameters allow us to confidently claim that actual force density exceeds the critical value for transverse flows and thus the latter could indeed be responsible for the coherent chromatin flows in live cells.

In the oscillatory regime, required critical force density is larger,  $f\rho/\zeta > (f\rho)^*/\zeta = (3a/\tau)[1 + (\eta^p/\eta^s)\lambda^2/R^2]$ ; see Eq. (8). Given the uncertainties in the estimates of  $\tau$  and ratio of viscosities, it is difficult at the present time to make definitive statements about feasibility of this regime for *in vivo* chromatin. A similar uncertainty exists about our predictions of running waves speed and oscillations period [Eq. (9)], which is poorly constrained, but seems significantly shorter than the measured lifetime of coherent chromatin flows in cells of  $\sim 5$ – $10 \text{ s}$  [7]. Importantly, a set of parameters consistent with current knowledge can be chosen that yields physiologically relevant results, yet such a choice cannot be presently motivated.

Overall, our model might be consistent with current measurements, although the significant approximations in our theory and uncertainties in parameters call for future efforts toward more detailed modeling. This will require consideration of the boundary conditions [46], including solvent permeation through the nuclear envelope [53], coupling of chromatin to lamin [54–56] and to nuclear envelope fluctuations [57]. Another promising direction is to account for a nonuniform distribution of active motors in the nucleus and along the chromatin fiber, such as active motors preferentially residing in transcriptionally active euchromatin [21,56,58]. But already now our theory makes predictions that beg for experimental tests, in particular for solvent motions, which unlike chromatin motions have not been measured before.

A. Z. is grateful for support from the NSF Grants No. CAREER PHY-1554880, No. CMMI-1762506, No. PHY-2210541, No. DMS-2153432, and No. NYU MRSEC DMR-1420073. This research was supported in part by the National Science Foundation under Grant No. NSF PHY-1748958. A. Z. and A. Y. G. acknowledge useful discussions with participants of the 2020 virtual KITP program on “Biological Physics of Chromosomes.” A. Y. G. thanks S. Ramaswamy for useful discussions.

---

\*Corresponding author.

ayg1@nyu.edu

- [1] K. Alberts, A. Johnson, J. Lewis, D. Morgan, M. Raff, K. Roberts, and P. Walter, *Molecular Biology of the Cell* (W.W. Norton, New York, 2017).
- [2] K. E. Van Holde, *Chromatin* (Springer Science & Business Media, New York, 2012).
- [3] R. Milo and R. Phillips, *Cell Biology by the Numbers* (Garland Science, New York, 2015).
- [4] T. Cremer and C. Cremer, Chromosome territories, nuclear architecture and gene regulation in mammalian cells, *Nat. Rev. Genet.* **2**, 292 (2001).
- [5] M. R. Hübner and D. L. Spector, Chromatin dynamics, *Annu. Rev. Biophys.* **39**, 471 (2010).
- [6] A. Zidovska, The self-stirred genome: Large-scale chromatin dynamics, its biophysical origins and implications, *Curr. Opin. Genet. Dev.* **61**, 83 (2020).
- [7] A. Zidovska, D. A. Weitz, and T. J. Mitchison, Micron-scale coherence in interphase chromatin dynamics, *Proc. Natl. Acad. Sci. U.S.A.* **110**, 15555 (2013).
- [8] R. Bruinsma, A. Y. Grosberg, Y. Rabin, and A. Zidovska, Chromatin hydrodynamics, *Biophys. J.* **106**, 1871 (2014).
- [9] D. Saintillan, M. J. Shelley, and A. Zidovska, Extensile motor activity drives coherent motions in a model of interphase chromatin, *Proc. Natl. Acad. Sci. U.S.A.* **115**, 11442 (2018).
- [10] M. C. Marchetti, J.-F. Joanny, S. Ramaswamy, T. B. Liverpool, J. Prost, M. Rao, and R. A. Simha, Hydrodynamics of soft active matter, *Rev. Mod. Phys.* **85**, 1143 (2013).

- [11] T. Vicsek, A. Czirók, E. Ben-Jacob, I. Cohen, and O. Shochet, Novel Type of Phase Transition in a System of Self-Driven Particles, *Phys. Rev. Lett.* **75**, 1226 (1995).
- [12] J. Toner and Y. Tu, Long-Range Order in a Two-Dimensional Dynamical XY Model: How Birds Fly Together, *Phys. Rev. Lett.* **75**, 4326 (1995).
- [13] R. A. Simha and S. Ramaswamy, Hydrodynamic Fluctuations and Instabilities in Ordered Suspensions of Self-Propelled Particles, *Phys. Rev. Lett.* **89**, 058101 (2002).
- [14] K. Kruse, J.-F. Joanny, F. Jülicher, J. Prost, and K. Sekimoto, Asters, Vortices, and Rotating Spirals in Active Gels of Polar Filaments, *Phys. Rev. Lett.* **92**, 078101 (2004).
- [15] A. Ahmadi, T. B. Liverpool, and M. C. Marchetti, Nematic and polar order in active filament solutions, *Phys. Rev. E* **72**, 060901(R) (2005).
- [16] F. C. Keber, E. Loiseau, T. Sanchez, S. J. DeCamp, L. Giomi, M. J. Bowick, M. C. Marchetti, Z. Dogic, and A. R. Bausch, Topology and dynamics of active nematic vesicles, *Science* **345**, 1135 (2014).
- [17] R. M. Adar and J.-F. Joanny, Permeation Instabilities in Active Polar Gels, *Phys. Rev. Lett.* **127**, 188001 (2021).
- [18] F. Jülicher, K. Kruse, J. Prost, and J.-F. Joanny, Active behavior of the cytoskeleton, *Phys. Rep.* **449**, 3 (2007).
- [19] A. C. Callan-Jones and F. Jülicher, Hydrodynamics of active permeating gels, *New J. Phys.* **13**, 093027 (2011).
- [20] Z. W. Zhao, R. Roy, J. C. M. Gebhardt, D. M. Suter, A. R. Chapman, and X. S. Xie, Spatial organization of RNA polymerase II inside a mammalian cell nucleus revealed by reflected light-sheet superresolution microscopy, *Proc. Natl. Acad. Sci. U.S.A.* **111**, 681 (2014).
- [21] G. Shi, L. Liu, C. Hyeon, and D. Thirumalai, Interphase human chromosome exhibits out of equilibrium glassy dynamics, *Nat. Commun.* **9**, 3161 (2018).
- [22] L. Liu, G. Shi, D. Thirumalai, and C. Hyeon, Chain organization of human interphase chromosome determines the spatiotemporal dynamics of chromatin loci, *PLoS Comput. Biol.* **14**, e1006617 (2018).
- [23] M. Di Pierro, D. A. Potoyan, P. G. Wolynes, and J. N. Onuchic, Anomalous diffusion, spatial coherence, and viscoelasticity from the energy landscape of human chromosomes, *Proc. Natl. Acad. Sci. U.S.A.* **115**, 7753 (2018).
- [24] I. Eshghi, A. Zidovska, and A. Y. Grosberg, Symmetry-based classification of forces driving chromatin dynamics, *Soft Matter* **18**, 8134 (2022).
- [25] M. Doi and A. Onuki, Dynamic coupling between stress and composition in polymer solutions and blends, *J. Phys. II* **2**, 1631 (1992).
- [26] See Supplemental Material at <http://link.aps.org/supplemental/10.1103/PhysRevLett.131.048401> for further technical details and derivations, which includes Refs. [3,9,20,24,27–43].
- [27] Y. Tseng, J. S. Lee, T. P. Kole, I. Jiang, and D. Wirtz, Micro-organization and visco-elasticity of the interphase nucleus revealed by particle nanotracking, *J. Cell Sci.* **117**, 2159 (2004).
- [28] F. M. Hameed, M. Rao, and G. Shivashankar, Dynamics of passive and active particles in the cell nucleus, *PLoS One* **7**, e45843 (2012).
- [29] A. Celedon, C. M. Hale, and D. Wirtz, Magnetic manipulation of nanorods in the nucleus of living cells, *Biophys. J.* **101**, 1880 (2011).
- [30] A. H. de Vries, B. E. Krenn, R. van Driel, V. Subramaniam, and J. S. Kanger, Direct observation of nanomechanical properties of chromatin in living cells, *Nano Lett.* **7**, 1424 (2007).
- [31] I. Eshghi, J. A. Eaton, and A. Zidovska, Interphase Chromatin Undergoes a Local Sol-Gel Transition upon Cell Differentiation, *Phys. Rev. Lett.* **126**, 228101 (2021).
- [32] C. M. Caragine, S. C. Haley, and A. Zidovska, Surface Fluctuations and Coalescence of Nucleolar Droplets in the Human Cell Nucleus, *Phys. Rev. Lett.* **121**, 148101 (2018).
- [33] L. Liang, X. Wang, X. Da, T. Chen, and W. R. Chen, Noninvasive determination of cell nucleoplasmic viscosity by fluorescence correlation spectroscopy, *J. Biomed. Opt.* **14**, 024013 (2009).
- [34] F. Erdel, M. Baum, and K. Rippe, The viscoelastic properties of chromatin and the nucleoplasm revealed by scale-dependent protein mobility, *J. Phys. Condens. Matter* **27**, 064115 (2015).
- [35] A. Zidovska, The rich inner life of the cell nucleus: Dynamic organization, active flows, and emergent rheology, *Biophys. Rev. Lett.* **12**, 1093 (2020).
- [36] A. J. Lotka, Contribution to the theory of periodic reactions, *J. Phys. Chem.* **14**, 271 (1910).
- [37] V. Volterra, Variations and fluctuations of the number of individuals in animal species living together, *ICES J. Mar. Sci.* **3**, 3 (1928).
- [38] H. Kimura, Y. Tao, R. G. Roeder, and P. R. Cook, Quantitation of RNA polymerase II and its transcription factors in an HeLa cell: Little soluble holoenzyme but significant amounts of polymerases attached to the nuclear substructure, *Mol. Cell Biol.* **19**, 5383 (1999).
- [39] S. M. Görisch, K. Richter, M. O. Scheuermann, H. Herrmann, and P. Lichter, Diffusion-limited compartmentalization of mammalian cell nuclei assessed by micro-injected macromolecules, *Exp. Cell Res.* **289**, 282 (2003).
- [40] I. Solovei, A. Cavallo, L. Schermelleh, F. Jaunin, C. Scasselati, D. Cmarko, C. Cremer, S. Fakan, and T. Cremer, Spatial preservation of nuclear chromatin architecture during three-dimensional fluorescence in situ hybridization (3D-FISH), *Exp. Cell Res.* **276**, 10 (2002).
- [41] P. J. W. Debye, *Polar Molecules* (Dover Publications, New York, 1929).
- [42] Y. Rabin and A. Y. Grosberg, Nanorheology of polymer solutions: A scaling theory, *Macromolecules* **52**, 6927 (2019).
- [43] P.-G. De Gennes, *Scaling Concepts in Polymer Physics* (Cornell University Press, Ithaca, NY, 1979).
- [44] N. Kumar, H. Soni, S. Ramaswamy, and A. Sood, Flocking at a distance in active granular matter, *Nat. Commun.* **5**, 4688 (2014).
- [45] P. Ahlrichs, R. Everaers, and B. Dünweg, Screening of hydrodynamic interactions in semidilute polymer solutions: A computer simulation study, *Phys. Rev. E* **64**, 040501(R) (2001).
- [46] I. Eshghi, A. Zidovska, and A. Y. Grosberg, Model chromatin flows: Numerical analysis of linear and nonlinear hydrodynamics inside a sphere, [arXiv:2305.02411](https://arxiv.org/abs/2305.02411).

- [47] It is useful to note parenthetically the following simple fact about signs: In spatial Fourier representation, while  $\nabla \nabla \cdot \mathbf{w} \rightarrow -q^2 \mathbf{w}$ , with minus sign, but  $\nabla \times \nabla \times \mathbf{w} \rightarrow +q^2 \mathbf{w}$ , with the sign plus.
- [48] B. van der Pol, A theory of the amplitude of free and forced triode vibrations, *London, Edinburgh, Dublin Philos. Mag. J. Sci.* **2**, 978 (1926).
- [49] A. A. Andronov, A. A. Vitt, and S. E. Khaikin, *Theory of Oscillators* (Dover Publications, New York, 2011).
- [50] M. Ganji, I. A. Shaltiel, S. Bisht, E. Kim, A. Kalichava, C. H. Haering, and C. Dekker, Real-time imaging of DNA loop extrusion by condensin, *Science* **360**, 102 (2018).
- [51] H.-Y. Wang, T. Elston, A. Mogilner, and G. Oster, Force generation in RNA polymerase, *Biophys. J.* **74**, 1186 (1998).
- [52] T. Rhodin, J. Fu, K. Umemura, M. Gad, S. Jarvis, and M. Ishikawa, Single molecule imaging of RNA polymerase II using atomic force microscopy, *Appl. Surf. Sci.* **210**, 105 (2003).
- [53] P. L. Paine, L. C. Moore, and S. B. Horowitz, Nuclear envelope permeability, *Nature (London)* **254**, 109 (1975).
- [54] Q. MacPherson, B. Beltran, and A. J. Spakowitz, Chromatin compaction leads to a preference for peripheral heterochromatin, *Biophys. J.* **118**, 1479 (2020).
- [55] M. Falk, Y. Feodorova, N. Naumova, M. Imakaev, B. R. Lajoie, H. Leonhardt, B. Joffe, J. Dekker, G. Fudenberg, I. Solovei, and L. A. Mirny, Heterochromatin drives compartmentalization of inverted and conventional nuclei, *Nature (London)* **570**, 395 (2019).
- [56] A. Mahajan, W. Yan, A. Zidovska, D. Saintillan, and M. J. Shelley, Euchromatin Activity Enhances Segregation and Compaction of Heterochromatin in the Cell Nucleus, *Phys. Rev. X* **12**, 041033 (2022).
- [57] F.-Y. Chu, S. C. Haley, and A. Zidovska, On the origin of shape fluctuations of the cell nucleus, *Proc. Natl. Acad. Sci. U.S.A.* **114**, 10338 (2017).
- [58] A. Goychuk, D. Kannan, A. K. Chakraborty, and M. Kardar, Polymer folding through active processes recreates features of genome organization, *Proc. Natl. Acad. Sci. U.S.A.* **120**, e2221726120 (2023).